CLIMATE SCIENCE

10.1126/sciadv.1500157

Natural aerosols explain seasonal and spatial patterns of Southern Ocean cloud albedo

Daniel T. McCoy,[1]*† Susannah M. Burrows,[2]*† Robert Wood,[1] Daniel P. Grosvenor,[3] Scott M. Elliott,[4] Po-Lun Ma,[2] Phillip J. Rasch,[2] Dennis L. Hartmann[1]

Atmospheric aerosols, suspended solid and liquid particles, act as nucleation sites for cloud drop formation, affecting clouds and cloud properties—ultimately influencing the cloud dynamics, lifetime, water path, and areal extent that determine the reflectivity (albedo) of clouds. The concentration N_d of droplets in clouds that influences planetary albedo is sensitive to the availability of aerosol particles on which the droplets form. Natural aerosol concentrations affect not only cloud properties themselves but also modulate the sensitivity of clouds to changes in anthropogenic aerosols. It is shown that modeled natural aerosols, principally marine biogenic primary and secondary aerosol sources, explain more than half of the spatiotemporal variability in satellite-observed N_d. Enhanced N_d is spatially correlated with regions of high chlorophyll a, and the spatiotemporal variability in N_d is found to be driven primarily by high concentrations of sulfate aerosol at lower Southern Ocean latitudes (35° to 45°S) and by organic matter in sea spray aerosol at higher latitudes (45° to 55°S). Biogenic sources are estimated to increase the summertime mean reflected solar radiation in excess of 10 W m^{-2} over parts of the Southern Ocean, which is comparable to the annual mean increases expected from anthropogenic aerosols over heavily polluted regions of the Northern Hemisphere.

INTRODUCTION

The Southern Ocean (SO) is an expansive and dynamic ocean with rich ecosystems remote from most human influences. It is also the cloudiest region on Earth. These clouds influence the atmospheric and oceanic circulation of the entire Southern Hemisphere and beyond (*1*), and may help determine the Earth's climate sensitivity (*2*). Its remoteness from anthropogenic and natural continental aerosol sources makes the SO a unique natural laboratory for our understanding of aerosol-cloud interactions. Aerosols influence clouds by acting as the cloud condensation nuclei (CCN) on which cloud droplets form, and the resulting concentration N_d of cloud droplets influences the amount of sunlight reflected by clouds (*3*). Aerosol processes remain a poorly understood influence on clouds (*4*). Processes regulating the concentration of naturally occurring aerosols, in particular, remain a major source of uncertainty, limiting our ability to quantify the magnitude of the human impact on climate from aerosols (*5*, *6*).

The rich biological activity in the SO produces a range of biogenic aerosols and aerosol precursor gases (*7*). Marine biogenic emissions influence atmospheric aerosols in this region, both through primary emissions of organic matter in sea spray aerosol (SSA) (*8*) and through secondary aerosol formation processes, that is, the condensation of volatile sulfurous and organic compounds (*7*–*9*). The effect of marine biota on clouds and climate through biogenic sulfate aerosol has been the subject of intense research for several decades (*10*). In recent years, primary organic aerosol species have received considerable attention as well (*8*). Chlorophyll a (Chl-a), a proxy for the phytoplankton biomass believed to be a source for aerosol and aerosol precursors, has been found to be negatively correlated with the radius of cloud droplets over the seasonal cycle in selected biologically active regions of the SO, indicating that aerosol originating from marine microbial communities may be associated with enhanced concentrations of CCN (*11*, *12*). Although previous investigations did much to probe the coupling between biological activity and clouds (*8*, *10*–*14*), they were limited in three ways. First, previous studies did not correct for seasonal biases in the remote sensing of cloud properties at high latitudes, which were unknown at the time. This conflated true seasonal variations in N_d due to CCN number with seasonal retrieval biases due to solar angle. Second, they did not examine the distributions of both primary aerosols and secondary sulfate aerosols from marine biota and their respective roles as mediators of the Chl-a–N_d correlation. Finally, most previous studies examined limited regions within the SO where strong seasonal cycles in Chl-a may correlate with underlying seasonal cycles in meteorological variables, confounding the detection of an unambiguous signal of phytoplankton effects on clouds.

The Moderate Resolution Imaging Spectroradiometer (MODIS) instrument on the NASA Terra satellite offers remotely sensed estimates of N_d with global coverage. In this work, we use a new MODIS N_d data set that eliminates certain retrieval biases (*15*), allowing for the first time the comprehensive study of the relationship between N_d and modeled marine biogenic aerosols over the entire SO. Biases due to seasonal-latitudinal variations in the solar zenith angle (SZA) affect the visible to near-infrared satellite retrievals of cloud optical thickness and droplet effective radius used by MODIS to estimate N_d. These biases are mitigated by removing all retrievals with SZA >65° (*15*).

RESULTS AND DISCUSSION

With this new data set, we find that spring-summer-autumn (September to April) mean that N_d values are elevated in the regions of the SO with the most active ocean biology as indicated by Chl-a (Fig. 1), demonstrating that ocean biology drives variations in N_d across the entire SO.

[1]Department of Atmospheric Sciences, University of Washington, Seattle, WA 98195–1640, USA. [2]Atmospheric Sciences Division, Pacific Northwest National Laboratory, Richland, WA 99352, USA. [3]School of Earth and Environment, University of Leeds, Leeds LS2 9JT, UK. [4]Climate Ocean Sea Ice Modeling team, Computational Physics and Methods group, Los Alamos National Laboratory, Los Alamos, NM 87545, USA.
*Corresponding author. E-mail: dtmccoy@atmos.uw.edu (D.T.M.); susannah.burrows@pnnl.gov (S.M.B.)
†These authors contributed equally to this work.

Correlations between N_d and candidate aerosols

It is interesting that a significant correlation is found between regions of high Chl-a and enhanced N_d; however, a more physical understanding of what drives the spatiotemporal variability in the SO necessitates investigation of the SO CCN amount and provenance. Unfortunately, remote sensing alone cannot determine the detailed chemical composition of aerosol. In particular, it cannot distinguish between sea salt (SS), sulfate, and organic aerosol because they all primarily scatter rather than absorb incoming radiation. To determine which aerosol species are responsible for driving the observed Chl-a–N_d relationship over the SO, we combine N_d observations with candidate aerosol products derived from global modeling to develop a regression model to predict N_d over the SO. Sulfate and SS surface concentrations are taken from the multimodel median year 2000 global model simulations performed for phase 1 of the AeroCom project (*16*). Aerosol modeling is extremely complex and subject to a great deal of uncertainty and, consequently, intermodel disagreement (*17*). Because of this diversity, the use of the AeroCom multimodel median data set is likely to provide a more robust representation of the distribution of an aerosol species than any single model. The non-SS aerosol candidates selected here, marine organic matter and SO_4, have been chosen on the basis of observational evidence for their efficacy as CCN. Sulfate aerosol is found to serve efficiently as a CCN (*18*, *19*), and in situ measurements in marine air have identified a contribution of organic aerosols to CCN (*20*). In the SO region, dust may be important as a source of ice nuclei (*21*, *22*) and oceanic micronutrients such as iron (*23*, *24*). However, dust sources in the Southern Hemisphere are minimal, and the mean contribution to the total aerosol number and CCN in the SO is small, particularly when compared to sea spray and sulfate aerosol. This has been established by satellite and in situ observations and is reflected in global chemistry-climate models (*17*, *25*–*31*). We will now discuss the inclusion of organic enrichment of SSA as a predictor variable.

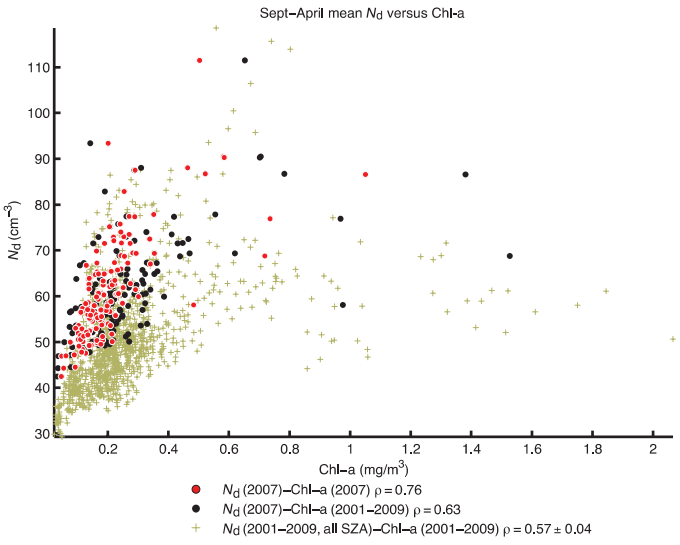

Fig. 1. Elevated mean September to April cloud droplet concentrations over the SO are associated with regions of high Chl-a (indicating the presence of phytoplankton biomass). Spring-summer-autumn (September to April) mean values of N_d are shown as a function of SeaWiFS Chl-a (for 5° latitude × 15° longitude boxes from 35° to 55°S). Three comparisons are shown: N_d from 2007 only using retrievals SZA <65° versus Chl-a from 2007 (red); N_d from 2007 (only retrievals with SZA <65°) versus a climatology of Chl-a from 2001 to 2009 (black); and N_d from each year from 2001 to 2009 (all retrievals) versus Chl-a from each year from 2001 to 2009 (brown). The Spearman rank correlations are 0.76, 0.63, and 0.57 ± 0.04, respectively, where the mean and SD of the latter is calculated from the individual correlations from each year from 2001 to 2009.

The mechanisms by which phytoplankton affect organic aerosol in the atmosphere are a subject of ongoing research and debate, and there is no consensus yet on the effect of marine phytoplankton and organic matter on the number, size, mixing state, and detailed organic chemistry of emitted particles. Model simulations of atmospheric transport and removal of aerosols, and of aerosol-cloud interactions, are extremely sensitive to the details of such assumptions in models, and differing choices may result in strong changes of the magnitude or even the sign of effects on CCN and N_d (*12*). Furthermore, although strong evidence supports the existence of a primary sea spray source of marine organic aerosol, the relative importance of condensational growth by secondary aerosol formation from marine precursor compounds is not well understood. However, a greater role for primary organics is suggested by evidence such as (i) the chemical similarity of aerosol generated at sea to ambient marine aerosol (*32*–*34*); (ii) single-particle measurements of marine organic particles, which show that these particles frequently contain solid fragments and agglomerates that cannot be explained by condensation (*35*–*37*); (iii) the correlation of wind speed with organic mass fraction (OMF) observed at sea in remote locations (*38*); and (iv) the observation that until now, most studies of which we are aware are able to demonstrate only a negligible to minor contribution to organic mass (OM) in naturally occurring marine aerosol from condensation of organic precursor gases [for example, oxalate (*39*, *40*) or isoprene (*41*)] or from atmospheric oxidation processes (*39*, *42*). Here, we use the OMF in emitted submicron SSA as a proxy for the effect of marine organic matter on primary SSA. OMF is calculated using OCEANFILMS, a physically based framework that models the enrichment of emitted primary sea spray particles with organic matter as being driven by adsorption of surface-active organics at the air-water interfaces of ocean bubbles, using fields from an ocean biogeochemical model to drive the analysis (*43*, *44*). Observational evaluation of the OCEANFILMS model shows skill in predicting OMF (*43*) despite inherent limitations in our ability to fully represent the complexity of ocean biogeochemistry (*45*). Although the OMF of emitted particles is not a direct estimate of aerosol number concentration, it has the virtue of not requiring additional assumptions to be made about the emissions process, for which observational support is not yet available. In particular, the effect on emitted number is a critical parameter needed by models to simulate the impact of marine organics on CCN number in models (*46*). We are unaware of firm observational evidence from field or laboratory studies that can inform models as to whether the total number and mass of SSA emitted increase, decrease, or remain the same in the presence of marine organics, although limited evidence suggests that total emissions may increase under some circumstances (*47*).

The OCEANFILMS parameterization is the first mechanistic model of the enrichment of organic matter in SSA appropriate for use in a global atmospheric model. An important feature of this model that distinguishes it from previous parameterizations of OMF is that it allows for a contribution to organic enrichment of SSA by classes of molecules whose spatial distribution is decoupled from that of Chl-a, namely, the polysaccharide- and protein-like classes of semi-labile organic macromolecules. This is particularly important in the nutrient-poor regions of the ocean, where Chl-a and primary productivity are low, but

longer-lived marine organic matter is imported by ocean currents from regions of high primary production. Observations show that for a given Chl-a concentration, marine aerosol organic enrichment in oligotrophic regions is higher than would be suggested by extrapolation from observations in mid-latitude bloom regions such as those in the North Atlantic (*32*, *47*–*49*).

The candidate aerosol products used as predictors for N_d are near-surface sulfate (SO_4) concentration, near-surface SS concentration, and OMF of emitted SSA. Additional candidate predictors considered are the surface wind speed, sea surface temperature (SST), ocean dimethyl sulfide (DMS) concentration (*50*), and Chl-a.

The relationships between N_d and the predictor variables were determined by multiple linear regression on monthly mean data averaged over 15° longitude × 5° latitude bins for those months where N_d retrievals are available. By using geographically binned monthly mean data, we improve signal-to-noise ratio and mitigate potential sampling biases related to the greater availability of usable retrievals. The uncertainty range in the variability in N_d explained by each set of predictor variables (R^2) was obtained using the 10-fold cross-validation (*51*) procedure repeated 10 times. The variability explained by each predictor is reported in Table 1. Individually, SO_4 and OMF are the two variables that explain the most seasonal and geographical variability in N_d, explaining 48 ± 7% and 35 ± 10%, respectively. These relationships are shown in Fig. 1. An increase in N_d with OMF (Fig. 1A) is found for high, intermediate, and low SO_4. Similarly, for a given concentration of SO_4, N_d generally increases with OMF (Fig. 2B). The SO_4 concentration and the OMF are only moderately correlated with each other (R^2 = 0.39), indicating the appropriateness of including both as independent predictors here. Only 9 ± 4% of the N_d variance is explained by SS, indicating that sea salt mass loading is not an important contributor to the spatial and seasonal variability in N_d over the SO during September through April. The variances explained in the spatial structure of the September to April N_d by SO_4 and OMF are 48 ± 24% and 33 ± 22%, respectively.

The multiple linear fit to both SO_4 and OMF explains 53 ± 6% of the variance in N_d, and the inclusion of additional aerosol-related predictors, including sea salt, did not significantly increase the explained variance. The total spatial variance in the September to April mean explained by OMF + SO_4 is 53 ± 22%. We find that monthly mean N_d as predicted by this regression is within 20% of observed N_d 74% of the time. The regression model of N_d is

$$N_d = \left(137 \pm 3\,\frac{\mathrm{cm^{-3}m^3}}{\mu g}\right)[\mathbf{SO_4}] + \left(58 \pm 2\ \mathrm{cm^{-3}}\right)\mathbf{OMF} + 36 \pm 0.2\ \mathrm{cm^{-3}} \quad (1)$$

where N_d has units of cm^{-3}, the surface SO_4 concentration has units of $\mu g\ m^{-3}$, and OMF is dimensionless. The constant term can be considered as the expected N_d over an ocean devoid of biological activity and is similar to aircraft measurements of N_d made off the coast of Tasmania (*52*) during winter, when biogenic aerosol sources are minimal.

Although this analysis cannot explicitly determine the composition of the CCN that determines background values of N_d (≈36 cm^{-3}), as estimated from the constant term in Eq. 1, it is likely that this background is largely attributable to SS. A detailed model study of CCN sources over the SO (*7*) found that SS contributed significantly, but the simulated number of CCN from SS was almost the same in summer and winter. As a result, SS explains little of the variance in N_d, but likely contributes to the constant term in the multiple linear regression. Under the assumption that the constant term is entirely attributable to SS, the summertime contribution of SS to N_d is about 55% and the wintertime contribution is near 80% in the 35° to 55°S region. As shown in Fig. 3, this is highly consistent with a previous model evaluation of the relative importance of SO_4 and SS as CCN in the SO, with a January

Table 1. The variability in N_d explained by each predictor. R^2 is given in percent for both unweighted calculations and a robust calculation using bi-square weights, using a bias-corrected N_d data set. Spatial R^2 values are calculated by applying the same regression procedure and using bi-square weights, but using time-averaged values of bias-corrected N_d for the period September through April. Additional notes following asterisks give the R^2 values calculated using a 9-year monthly climatology of MODIS N_d including retrievals at all SZAs. Uncertainties are the SDs of estimates of R^2 from 10-fold cross-validation, repeated 10 times.

	R^2 (%)	R^2 (robust, %)		Spatial R^2
OMF	24 ± 5	35 ± 10	*(14 ± 4, 16 ± 4)	33 ± 22
SO_4	45 ± 7	48 ± 7	*(20 ± 6, 23 ± 7)	48 ± 24
OMF + SO_4	49 ± 5	53 ± 6	*(22 ± 6, 28 ± 7)	53 ± 22
OMF + SO_4 + SS + wind	49 ± 6	53 ± 5		57 ± 20
OMF + SO_4 + SS	49 ± 6	53 ± 7		58 ± 22
SS	11 ± 4	9 ± 4		16 ± 17
SST	4 ± 3	3 ± 2		13 ± 13
Wind	14 ± 4	13 ± 3		18 ± 18
SS + wind	14 ± 4	13 ± 4		14 ± 13
SST + wind + SS	16 ± 5	17 ± 4		16 ± 13
Chl-a	20 ± 7	35 ± 13		55 ± 24
DMS	15 ± 6	19 ± 6		12 ± 11

contribution from SS of 48% at 30° to 45°S, 58% at 45° to 60°S, and a wintertime contribution of >80% at 30° to 45°S and >90% farther south (*7*).

Because the modeled sulfate concentration, the modeled OMF, and the satellite data do not represent the same years, our analysis cannot capture interannual variability in clouds or ocean biota. As seen in the observed correlation between Chl-a and N_d, the correlation decreases significantly when a climatology of Chl-a is used instead of the Chl-a observed in the same year as the N_d data (Fig. 1), suggesting that matching of the exact location, timing, and strength of phytoplankton blooms can improve the correlation between the presence of oceanic phytoplankton and cloud properties. This suggests that the predictive capability of the regression model in Eq. 1 might also be further improved by better representation of the interannual variability of simulated

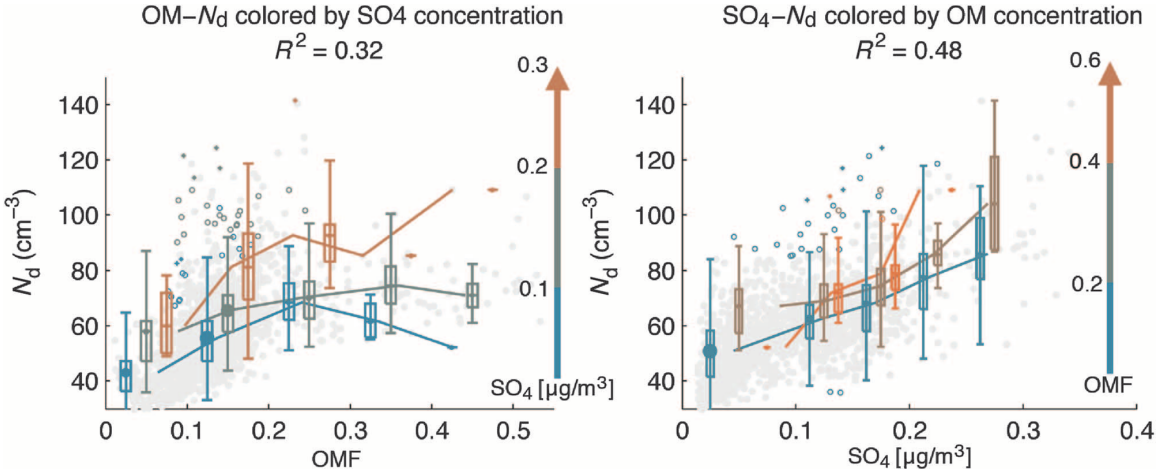

Fig. 2. Monthly mean N_d correlates with OMF and SO_4 concentration. Data points are given as gray dots. Box and whisker plots show binned means, boxes show interquartile range, whiskers show twice interquartile range, and outliers are shown as colored circles. Left: N_d as a function of OMF. Box and whisker plots are shown for three levels of SO_4 concentration. Higher SO_4 surface concentrations (orange) are associated with higher N_d for the same OMF. Right: N_d as a function of SO_4 surface concentration. Box and whisker plots are shown for three different bins of OMF, where higher OMF (orange) is associated with higher N_d for a given SO_4 concentration. All data are averaged monthly and over 5° × 15° boxes. R^2 values are shown for linear regressions between N_d and the respective predictor variable.

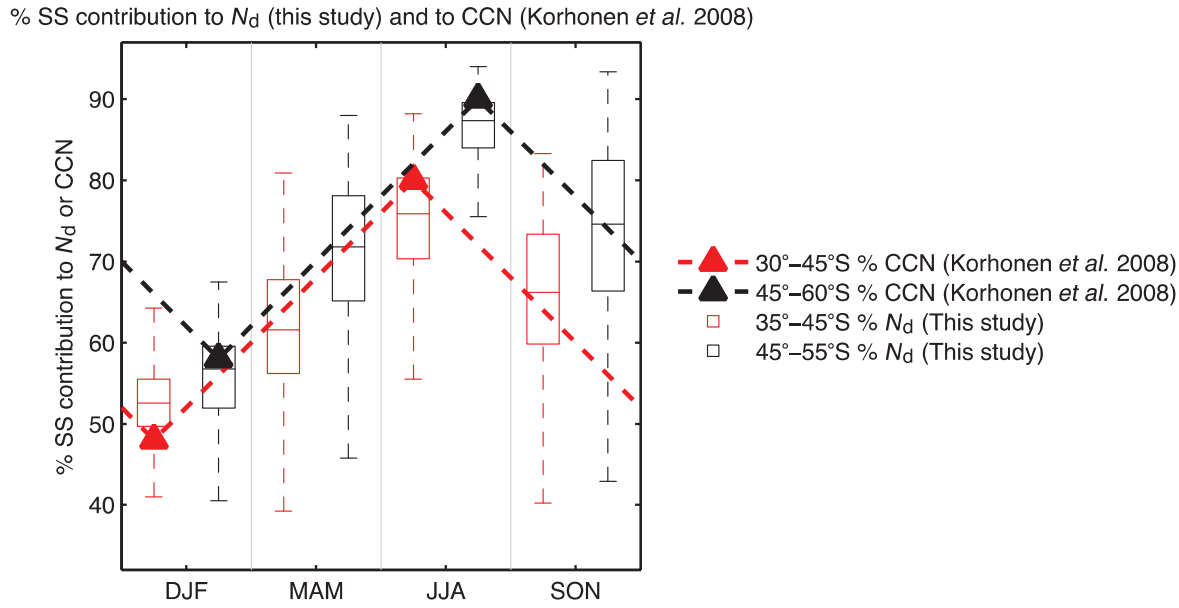

Fig. 3. Comparison of the fractional contributions to CCN from SS as estimated from this study and as modeled in the global aerosol model GLOMAP (*7*). The percentage contribution of SS to sulfate and SS CCN is estimated in this study as the constant term in Eq. 1 divided by the sum of the sulfate and constant terms from Eq. 1. The winter and summertime contributions of SS to CCN modeled by GLOMAP are shown in the figure with triangles, and the dashed connecting lines are provided as guides to the eye. The SS contributions from this study (oceans only) are shown aggregated into summer, fall, winter, and spring seasons and into 35° to 45°S and 45° to 55°S.

ocean biological activity and that the estimate of the explained variance due to OMF and SO_4 offered in this work is conservative.

The spatial structures of observed and predicted September to April mean N_d agree well (Fig. 4, A and B). Contributions to N_d from SO_4 (Fig. 4C) and OMF (Fig. 4D) determined from the regression model indicate that the impact of sulfate on summertime N_d is greater at lower SO latitudes (35° to 45°S), whereas the OMF contribution is more heterogeneous and spread over a broader range of latitudes with the major patches confined to higher latitudes (45° to 55°S). The seasonal cycle of N_d (Fig. 4F) shows a strong summertime peak in agreement with in situ measurements of CCN in the SO (*53*). Comparison of observed N_d (Fig. 4A), which shows a mean modeled N_d of 59 cm^{-3}, with the background for a biologically inactive ocean $N_d \approx 36$ cm^{-3}, suggests that ocean biology increases N_d by about 60% on average during September to April (spring-summer-autumn).

The highest SO_4 concentrations occur primarily at lower latitudes, whereas high OMF is found at all latitudes. Sunlight is required to oxidize DMS, and continental sources of natural sulfate aerosol are also stronger at lower latitudes (*7*). The sulfate sources affecting the northern SO (35° to 45°S) potentially have a significant volcanic component (*54*), in addition to the DMS sources of sulfate which dominate at higher latitudes (*54*–*56*). Anthropogenic emissions contribute less than a third of the SO_4 concentration on the annual mean over the study region, with a peak contribution to SO_4 of 35% at 35°S rapidly declining to 10% at 45°S; this is consistent with estimates of the DMS contributed SO_4 in this region provided by dedicated aerosol tagging studies (*56*). The N_d pattern is consistent with attributing much of the variability in N_d in the 35° to 45°S latitude band to sulfate (Fig. 4D). Organics in SSA contribute strongly in regions of high Chl-a (such as off the eastern coast of South America).

Increases in reflected shortwave radiation

These results imply that natural aerosols have the potential to significantly affect cloud droplet concentration over the SO. Observational estimates have shown that cloud microphysical processes can significantly affect the strength of the enhancement in cloud albedo with warming in the SO (*57*). Thus, accurate representation of natural, non-SS aerosols is likely to be important not only for accurate representation of the SO albedo in the current climate by global climate models (GCMs), which is generally too low (*2*), but also to help determine the strength of the optical depth feedback as the climate warms. Here, we quantify the effect of sulfate and primary organic aerosols on reflected shortwave (RSW) radiation, estimated in two ways: (i) from observed cloud properties and radiation (*11*), and (ii) using an offline radiative transfer calculation performed in Community Atmosphere Model version 5.3.38 (CAM5) using Portable Offline Radiative Transfer (PORT) (*58*). These calculations consider only the impact of changing N_d on RSW (the cloud albedo effect). Other aerosol effects, such as direct forcing, the cloud lifetime effect, and the semidirect effect, are not considered. We find that the increase in RSW from biogenic aerosol effects on N_d (Fig. 5A) exceeds 10 W m^{-2} during summer. Although the latitude range of the observed N_d data is limited by the range of SZAs at which a measurement can be made, the OMF and SO_4 data are modeled globally, and thus we may use them to extend the geographic range of our estimate of increased RSW to 70°S. This is especially interesting because of the increase in phytoplankton, and consequently OMF and RSW, at high latitudes during the summer as insolation increases and sea ice recedes (Fig. 5B). Although the sulfate contribution to the summertime increase in RSW is larger than that from OMF over the SO as a whole, both are found to be important. Another interesting finding is that enhanced RSW from OMF is often stronger than the contribution from SO_4 at high latitudes (Figs. 4 and 5). This suggests that detailed in situ observations of aerosol physical and chemical properties in combination with measurements of aerosol precursors and cloud properties may be able to distinguish the contributions from these two important species.

Previous studies have estimated the effect on annual mean RSW of sulfates from DMS emissions at 16 W m^{-2} over the SO in summer (*59*) and the effects of the observed seasonal cycle of effective radius, hypothesized to be due to biogenic aerosols, at 6 to 8 W m^{-2} during summer in the 40° to 60°S region (*60*). Here, the annual mean contribution to reflected shortwave (SW) is estimated to be between 4 and 6 W m^{-2} at 40°S with decreasing contributions poleward, and the summertime contribution is 6 to 10 W m^{-2} (Fig. 5D). This is comparable to the annual mean radiative forcing from aerosol-cloud interaction downwind of highly polluted regions as simulated in GCMs (*55*, *61*). It is also interesting to note that the bias in absorbed SW in the SO between 30° and 50°S in CMIP3 (*2*) is similar to the effect of SO_4 and OMF on RSW as estimated here. Given the significant enhancement in RSW estimated here, a detectable signature in cloud albedo should be evident from remote sensing. Recent studies have revealed a pattern of cloud albedo enhancement that is strikingly similar to the pattern of enhanced N_d described by this study, indicating the robustness of our results (*62*).

Possible pathways of enriched sea spray influence on N_d

While in situ studies have shown that organic aerosols can affect CCN (*20*) and our results indicate that organic matter in SSA over regions of high Chl-a affects N_d, there is no broad consensus on the mechanisms that generate these relationships. Some studies suggest that the presence of marine surfactants enhances the number of particles emitted in the range of diameters (roughly 50 to 200 nm) that are activated to form the majority of cloud droplets in the marine boundary layer (*47*, *63*). Aerosol chemistry is likely to be altered by biological activity, both through primary aerosol emissions and through condensation of biogenic volatile organic compounds, and experimental studies show that increases in the organic fraction in sea spray particles with diameters less than 180 nm correlated with increased biological activity (*63*, *64*). Another possibility is that secondary organic material condenses onto the primary spray particles, growing the smallest of them into CCN active sizes (*11*). Other observations suggest that although SSAs containing high fractions of organic material exhibit low hygroscopic growth at subsaturated relative humidities, they may nevertheless serve effectively as CCN under supersaturated conditions, possibly due to the surface activity of the organic matter (*65*). Surface-active organic material can reduce the aerosol surface tension, leading to a lowering of the critical activation radius and enhancing activation. Even comparatively weakly surface-active organic substances can facilitate droplet activation when they make up a large fraction of aerosol mass (*66*), as has been observed downwind of strong phytoplankton blooms (*67*, *68*). A fifth possibility is that the presence of a condensed film kinetically inhibits aerosol water uptake and growth, thereby delaying droplet formation (*69*). In the absence of a sufficient concentration of more efficient CCN, high supersaturations may be reached, ultimately allowing the activation of a larger proportion of the aerosol population. Finally, the mixing state of the aerosol may also evolve under the influence of biological changes to ocean chemistry, affecting CCN number (*70*).

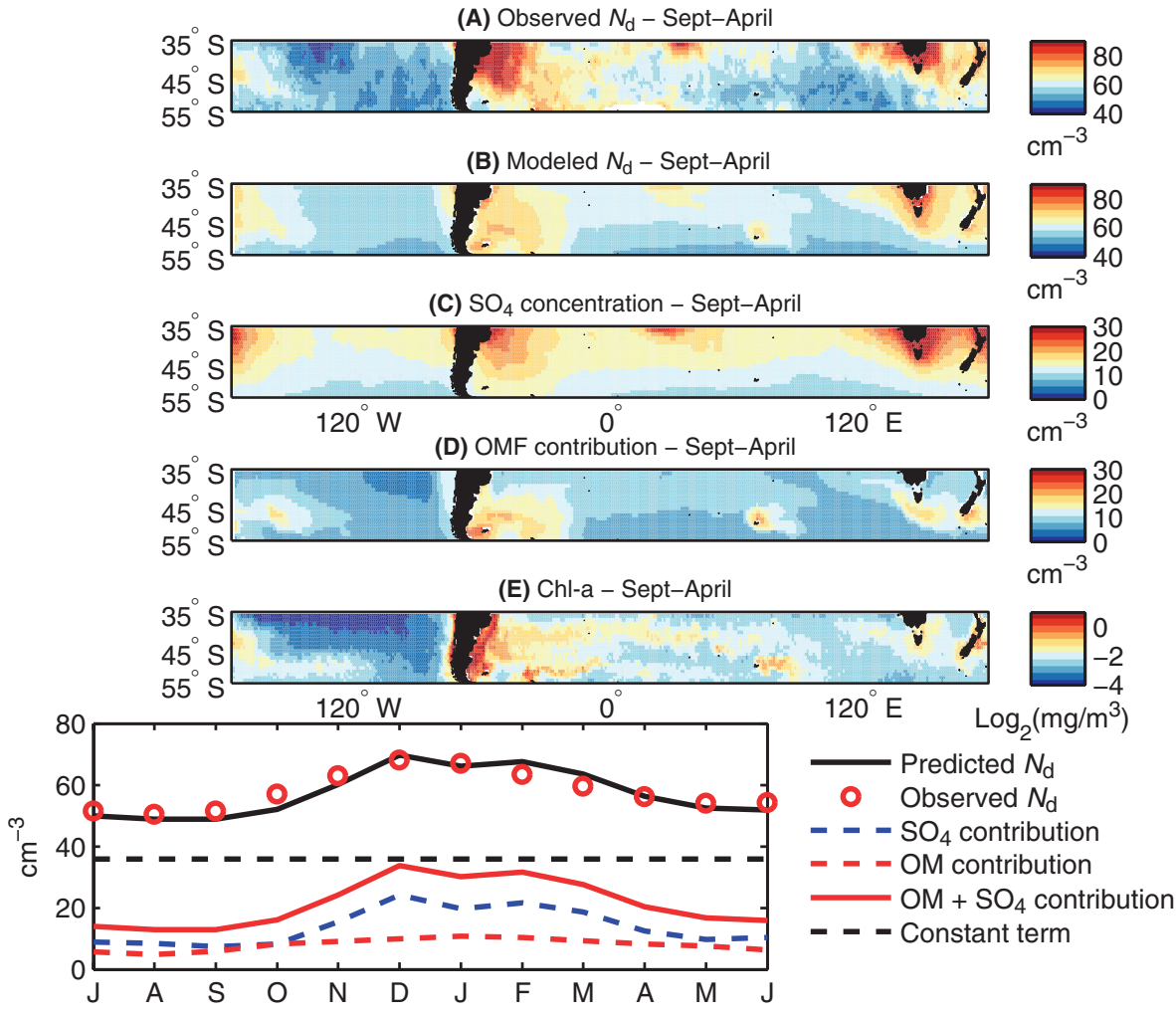

Fig. 4. The model captures significant spatial and seasonal structure in the SO N_d. (**A**) One year of N_d observations averaged from September through April (when observations are available for all months at all latitudes). (**B**) Predicted N_d from the regression model. (**C** and **D**) Contributions from OMF and SO_4 (note the different color scale). The means and spatial SDs are shown above each panel. The correlation between modeled and observed September-April mean N_d is $r = 0.71$, and the correlation between the September-April mean OMF and SO_4 contributions to N_d is $r = 0.41$. (**E**) Mean ocean Chl-a observed by SeaWiFS. (**F**) Time series of the observed N_d, modeled N_d, and the contributions of OMF, SO_4, their sum, and the constant term to N_d. Time series data are monthly averages over all locations where N_d is observed.

CONCLUSIONS

Here, we present observational data indicating a significant spatial correlation between regions of elevated Chl-a and N_d across the SO, and show that modeled OMF + SO_4 explains 53 ± 22% of the spatial variability in observed N_d. Further, a spatial and temporal correlation is shown relating observed N_d to modeled SO_4 and SSA organic enrichment, where the SO_4 is likely to be significantly biogenic. The regression model captures a large fraction, 53 ± 6%, of the spatial and seasonal variability in N_d, demonstrating that distributions of natural aerosols simulated by present-day climate models have sufficient fidelity to be useful in predicting climatological cloud properties over the SO. Because of the complexity of chemical and physical interactions affecting sea spray production and processing in the atmosphere, experimental and observational studies have been unable to unambiguously determine whether marine organic aerosol derived from phytoplankton is associated with an increase or with a decrease in CCN and N_d in marine clouds. The results of this study will inform future modeling of these processes by providing the first top-down estimate of the sign and magnitude of the impact of marine biogenic aerosol on N_d across the entire SO.

Our results suggest that ocean biology augments the cloud droplet concentration over the biologically active SO by about 60% in the annual mean and likely doubles it during summer when the incident solar radiation is strongest. The enhancement in upwelling SW due to these changes in cloud droplet number concentration is between 4 and 6 Wm^{-2} annually averaged and exceeds 10 W m^{-2} in summer. Accurate representation of the biogenic contribution to CCN and N_d over the oceans is therefore necessary for the accurate representation of climate forcing from aerosol-cloud interactions. To represent these processes in a changing climate will require models capable of representing the dynamic response of ocean biology to the warming and acidification of the oceans

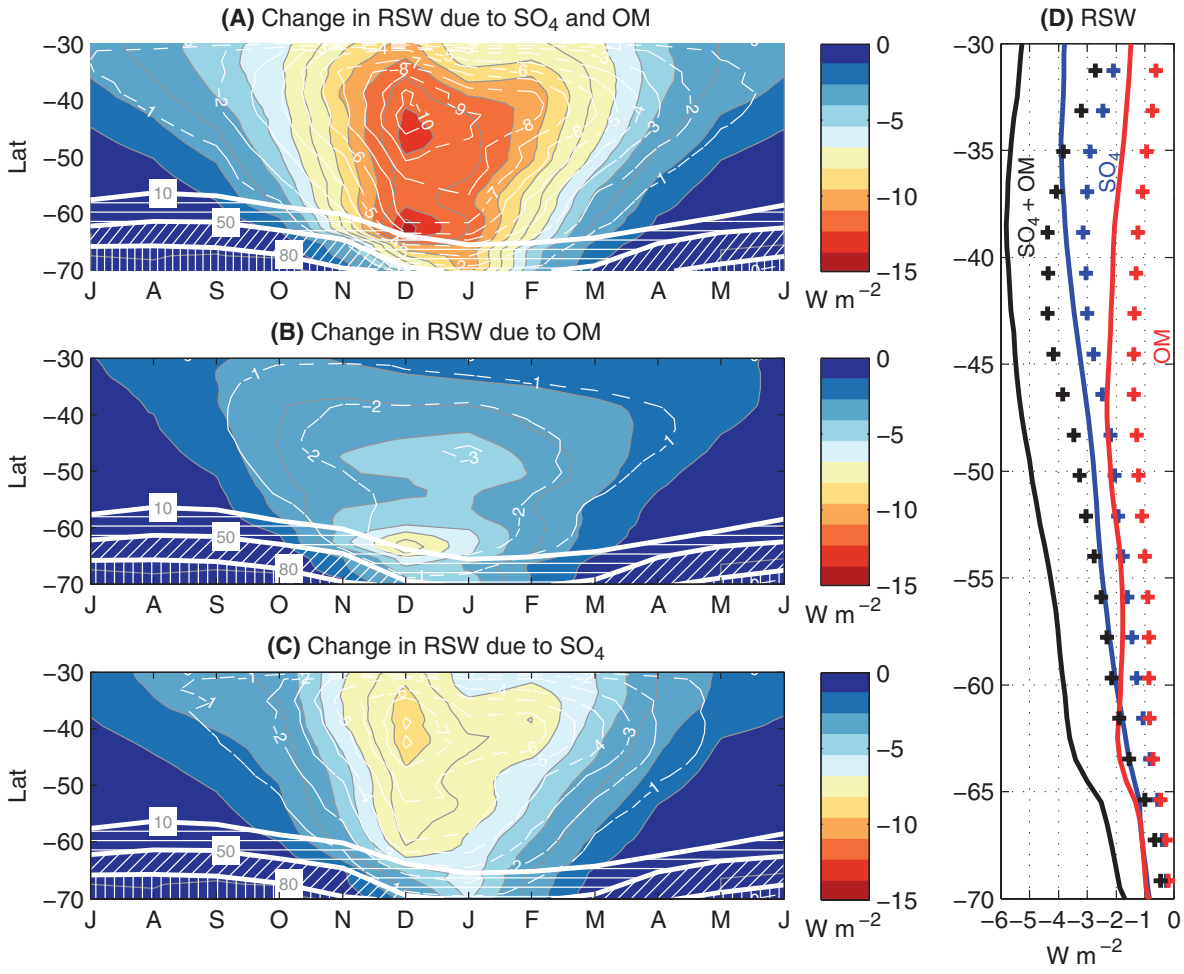

Fig. 5. OMF and SO_4 significantly affect SO cloud albedo. (**A** to **C**) Contours show the zonal mean change in top-of-atmosphere (TOA) net shortwave radiation (RSW) due to modification of N_d by (A) SO_4 and OMF, (B) OMF alone, and (C) SO_4 alone. (**D**) The annual mean contribution from OMF, SO_4, and the combination of OMF and SO_4. In (A) to (C), filled contours show the analytical estimate of the change in RSW based on observed cloud properties, and dashed white lines show the change in RSW calculated by an offline radiative transfer model using simulated cloud properties. Contour intervals are 1 W m^{-2} for both. Hatched white lines show the observed zonal mean sea ice extent (in percent). (D) Annual mean changes in RSW from the analytical estimate (solid lines) and the offline radiative transfer model (crosses).

and to the retreat of sea ice and predicting the subsequent effects on natural aerosol sources.

MATERIALS AND METHODS

Calculation of upwelling SW changes due to biogenic aerosol-cloud interactions

Meskhidze and Nenes method. The enhancement in upwelling shortwave radiation (RSW) caused by increases in N_d was estimated using the following equation, consistent with previous studies (*11*),

$$\Delta F = -\frac{1}{3} F_{in} A_c R_c (1 - R_c) \Delta \ln N_{db}$$

where ΔF is the change in RSW, F_{in} is the downwelling SW at cloud top, A_c is the monthly MODIS cloud fraction, R_c is the monthly MODIS cloud albedo, $\Delta \ln N_{db}$ is the change in N_d versus the background concentration $\Delta \ln N_{db} = (N_d - N_b)/N_d$, and N_d and N_b are the perturbed and background N_d, respectively.

Monthly, gridded observations of cloud properties, sea ice, and radiation from 2007 were used in the calculation of changes in RSW, excluding land surfaces. Cloud albedo was estimated from the MODIS cloud optical depth using the cloud albedo approximation of Lacis and Hansen (*71*). Cloud fraction was taken from MODIS, and downwelling SW at cloud top was approximated by the Clouds and Earth's Radiant Energy Systems (CERES) Energy Balanced and Filled (EBAF) 2.8 downwelling clear-sky SW at the surface. Sea ice distributions were taken from HADISST (Hadley Centre Sea Ice and Sea Surface Temperature) as included in the NOAA (National Oceanic & Atmospheric Administration) Optimum Interpolation (OI) SST, and the cloudy fraction of each grid box was assumed not to contribute to changes in RSW if clouds were over sea ice (*72*). Maximum overlap between sea ice and MODIS cloud fraction was assumed, resulting in a conservative estimate of the change in RSW in the presence of ice.

The N_d resulting from the presence of natural aerosols was calculated using the AeroCom sulfate concentration and B14 OMF data in combination with the regression detailed in the article (Eq. 1). The impacts of SO_4 and OMF + SO_4 on the TOA SW forcing were estimated as the change in RSW when N_d was increased from the background term in Eq. 1 to include the SO_4 term, OMF term, and their combination.

PORT method. Offline radiative transfer calculations were performed using the PORT tool (*58*) within the stand-alone CAM, which is the atmosphere component of the Community Earth System Model (CESM) (*73*). Details can be found online (www.cesm.ucar.edu/models/cesm1.0/cam/). Model simulations were performed using the CAM5 physics package (*74*). The model was compiled in an atmosphere-only configuration with prescribed ocean and ice boundary conditions with 1.9° × 2.5° grid spacing. CAM5 uses the Rapid Radiative Transfer Model for General circulation models (RRTMG) (*75*) to compute the radiative forcing of aerosols, clouds, and gases.

To obtain samples of the atmospheric state, instantaneous values of atmospheric state variables required for calculation of radiative transfer were recorded during a 2-year simulation (beginning 1 January 2000), of which the first year was discarded, allowing ample time for model spin-up. Atmospheric state variables were sampled every 73 model time steps, which corresponds to 1.5 days + 1 time step. This sampling frequency has been found to produce a representative sample of diurnal and seasonal cycles while reducing the computation cost of the calculation (*58*).

After the time samples were produced, the cloud drop size distribution of the time samples was then modified to correspond to each of three regression cases: background, background + SO_4, and background + SO_4 + OMF (described in point 3 below) for the subsequent PORT calculation. All other atmospheric state variables remained unchanged; therefore, changes in radiative forcing reflect changes in the cloud drop number concentration and related changes in cloud drop size distribution only, with no feedbacks onto cloud lifetime, atmospheric dynamics, or other processes.

The modification of the cloud drop size distribution was performed by the following procedure:

1. Calculate Nd_{inst_cldtop}, the cloud drop number concentration at cloud top (in each column), using the value of the in-cloud droplet number concentration that is passed to the radiation code. Cloud top was defined as occurring in the highest model layer in which the stratus cloud liquid water mixing ratio (*icwmrst*) was greater than 1×10^{-6} kg/kg.

$$Nd_{inst,cldtop}[cm^{-3}] = Nd_{inst}[\text{where}$$

$$icwmrst > 1 \times 10^{-6} kg/kg] \times \rho / 1 \times 10^{-6}$$

where ρ is the atmospheric density.

2. Calculate the climatological monthly mean of the cloud top droplet concentration ($Nd_{inst,cldtop}$) over the entire 5-year time series:

$$Nd_{month,cldtop} = \text{clim\_month\_ave}(Nd_{inst,cldtop}).$$

3. Calculate Nd_{reg}, the cloud top droplet number concentration as predicted from the regression model (Eq. 1), for each of three cases: (i) FULL: with all terms; (ii) SO4_BKGD: with coefficient of OMF term set to zero; (iii) BKGD_ONLY: with coefficients of SO_4 and OMF terms set to zero (constant term only).

The following steps are performed separately for each regression case.

4. Update the cloud drop number concentration in each column by multiplying by the ratio of the cloud top values of Nd from the regression and from the monthly mean:

$$Nd_{new} = Nd_{inst} \times Nd_{cldtop\_reg} / Nd_{cldtop\_month}.$$

5. Constrain Nd_{new} to be in the range [min[Nd_{inst}], max(Nd_{inst})] on a per-model-level basis:

$$\text{do lev} = 1,30$$

$$Nd_{new} = \min(Nd_{new}, \max(Nd_{inst}))$$

$$Nd_{new} = \max(Nd_{new}, \min(Nd_{inst}))$$

$$\text{end do}.$$

Similarly, constrain Nd_{new} so that the grid mean value (as opposed to the in-cloud value) of Nd is within the range of values in the original simulation (on a per-level basis).

6. Calculate new gamma parameters (rad_μ, rad_λ) using Nd_{new} and instantaneous values of air density (RHO) and stratus cloud fraction (AST). This calculation is identical to the calculation in the microphysics (*76*). Write out the updated values of rad_μ, rad_λ to the PORT input files.

Finally, PORT was run using the modified CAM history files to provide inputs to the offline radiative transfer code. This produces a new set of instantaneous history files that include the TOA radiation terms (upward, downward, and net, for SW and longwave radiation).

Estimation of anthropogenic component of SO_4 in the remote SO

Although the relative contributions of volcanoes and DMS are difficult to quantify, models indicate that near-surface sulfate over the SO is primarily from natural sources, with a peak biogenic contribution in the summer (*54*–*56*, *77*). Here, SO_4 is represented by the present-day surface concentration from the AeroCom A phase 1 multimodel median product. This includes SO_4 from volcanic, biogenic, and anthropogenic sources. Because simulated aerosols are not routinely tagged according to their sources in standard atmospheric model simulations, estimation of the volcanic component of the SO_4 would require a dedicated simulation (*56*). The volcanic contribution cannot be determined post hoc for the AeroCom product; however, previous studies have indicated that biogenic sulfate is the source of the majority of SO_4 over the SO poleward of 45°S, with increasing volcanic contributions northward of this latitude (*55*, *56*).

AeroCom phase 1 included three experiments: A (models are run with their native, present-day emissions), B (all models use the same, present-day emissions), and PRE (all models use the same, preindustrial emissions). Here, AeroCom A has been used to represent the present-day aerosols. Although the DMS emission inventories used in the AeroCom median are relatively similar, which leads to a lower model diversity in the case of SO_4 emissions (*78*), it incorporates a wider range of aerosol emissions, and thus, its median is hoped to represent the most diversity. On the other hand, this diversity makes it difficult to estimate anthropogenic increases in sulfate because the preindustrial and scenario A experiments do not use consistent emissions, so differences between the two may be either anthropogenic or natural (*28*).

Scenarios B and PRE have identical natural emissions, and their anthropogenic emissions are scaled with population size, crop production,

and wood consumption (*28*). Thus, differences between scenario B and PRE are purely anthropogenic and provide an approximation of the total present-day anthropogenic aerosol contribution (because preindustrial anthropogenic sources are small). Changes in SO_4 column density and surface concentration are shown in figs. S1 and S2, respectively. It can be see that in the eight models within the AeroCom median (all except MPI-HAM), for which SO_4 column density data were available, the anthropogenic contribution to loading is relatively minor and ranges between 10 and 20%; however, column density is not the variable examined in this study, and it is expected that near-surface SO_4 will be significantly less affected by anthropogenic emissions (*77*). The four models considered in the AeroCom phase 1 median data set (LSCE, GISS, LOA, and UIO-GCM) for which near-surface SO_4 concentration was available in the preindustrial data show that the increase in SO_4 from preindustrial to present day is relatively small over the SO (fig. S3). The mean fractional contribution of industrial-era anthropogenic SO_4 is at most 35% (at 35°S) and is 10% or less at latitudes south of 45°S (fig. S4), indicating that the majority of sulfate in the remote SO is natural, rather than anthropogenic.

Description of OMB14 (OCEANFILMS) parameterization and contributions of different components of marine OM to total OM

The recently developed OCEANFILMS (*43*) parameterization is the first mechanistic model of the enrichment of organic matter in SSA appropriate for use in a global atmospheric model. Enrichment is modeled as competitive physical adsorption of several classes of marine organic matter onto bubble surfaces, including a lipid-like class (LIPID) that is strongly associated with fresh primary production, and polysaccharide-like (POLY) and protein-like (PROT) classes that are associated with semi-labile dissolved organic matter with a modeled chemical lifetime of 100 days.

Marine biota and organic matter concentrations are simulated by the Biogeochemical Ecosystems Cycling (BEC) model within the Parallel Ocean Program (POP) (*43*). The BEC model has recently been optimized and evaluated against an extensive set of marine organic matter measurements (*44*). The distributions of macromolecular classes used in OCEANFILMS are derived by association with biogeochemical variables as calculated by BEC, including phytoplankton and zooplankton concentrations (LIPID), and semi-labile dissolved organic carbon (DOC) (POLY and PROT). The chemical properties of these classes and their propensity to adsorb to the air-water interface are estimated from the properties of well-studied proxy molecules. A more detailed evaluation of the ocean concentrations of the macromolecular classes is in progress (Ogunro *et al.,* 2015, in revision). In an initial evaluation, the parameterization has been shown to agree reasonably well with observations of the OMF of SSA in clean marine air from both shipboard and coastal clean-marine measurements, as well as with spray generated at sea. The OMF distributions used here are based on the 33rd year of a free-running simulation initialized in the year 2000.

A unique feature of the OCEANFILMS model is its treatment of marine organic matter as a sum of several broad classes of marine macromolecules. The spatial variability in the model's total OMF is almost entirely determined by two components: a "lipid-like" labile portion that is strongly associated with regions of primary productivity and highly correlated with Chl-a (LIPID), and a semi-labile portion with a model lifetime of 100 days ("polysaccharide-like"/POLY and "protein-like"/PROT classes). The R^2 values for regressions of N_d against individual classes (LIPID and POLY) are given in table S1. Breaking down the total organic fraction into these two components reveals differences in the spatial patterns of their contribution to N_d (fig. S5). The labile LIPID group contributes much more in the immediate vicinity of phytoplankton blooms (as indicated by Chl-a) than in oligotrophic regions. The total semi-labiles, POLY + PROT, contribute more in the northern part of the domain (35° to 45°S), and their contribution is less variable in both space (fig. S5) and time (not shown). The inclusion of the POLY + PROT fraction therefore reduces the overall spatiotemporal variability of OMF and of its effect on N_d in the regression model. Additional details about the OMF simulation can be found in the paper describing the parameterization (*43*).

Comparison of OMB14 to observationally derived parameterizations of OMF

The work of Burrows *et al.* (*43*) (B14) is different from previous methods of parameterizing the submicron SSA OMF in that it is a physically based framework as opposed to an empirical relationship derived from observations of Chl-a and OMF.

To assess whether parameterizations of OMF based on Chl-a can better predict N_d, B14 is compared to two such parameterizations (*49*, *79*). The latter study [Gantt *et al.* (*79*)] includes empirical fits to data from both the Mace Head Atmospheric Research Station (53.33°N, 9.9°W) and Point Reyes National Sea Shore (38.12°N, 122.91°W). To evaluate if B14 significantly improves on empirical parameterizations, OMF consistent with each empirical fit was calculated using the POP/BEC ocean biogeochemistry-simulated chlorophyll rather than observed chlorophyll, to provide a fair comparison with B14. Because ocean biology will respond to future changes in ocean temperature, acidity, and sea ice extent, it is important to evaluate how well parameterizations can perform within the context of simulated ocean biology, which can dynamically change in response to ocean conditions. The correlations of N_d with the OMF calculated using each of these parameterizations or the POP Chl-a fields is low, with less than 20% of the variance explained by any of the parameterizations. By contrast, B14 explains 37 ± 10% of the variance in N_d as a single predictor (fig. S6). This is because B14 includes components driven by two categories of ocean biological variables with differing spatial and seasonal distributions: a "lipid-like" component that is strongly correlated with Chl-a and a "polysaccharide-like" component that is tied to the longer-lived semi-labile DOC, whose distribution is simulated by POP/BEC.

The prediction of biogeochemistry is challenging, and the BEC ocean model predicts a different distribution of Chl-a than is observed by SeaWiFS (Sea-Viewing Wide Field-of-View Sensor) (*45*). It is likely that the simulation of OMF by B14 is limited by the oceanic biogeochemistry model's accuracy. To estimate the degree to which the B14 OMF might be improved by a more accurate simulation of oceanic biology, a relationship between Chl-a and the B14 lipid mass fraction has been derived using POP/BEC Chl-a (fig. S7). This relationship is used to calculate a distribution of the lipid-like class that is consistent with SeaWiFS-observed Chl-a.

The variance explained by OMF is calculated for several common empirical functions of Chl-a (*49*, *79*). This is compared to the variance explained by OMF calculated by B14. Two cases are considered: Chl-a as observed by SeaWiFS and as simulated by the POP/BEC model. In both cases, the OMF consistent with the empirical parameterizations is calculated on the basis of Chl-a. In the former case, the B14 analogous OMF is calculated using the combination of polysaccharide-like OMF calculated from the POP/BEC model and lipid-like OMF calculated using SeaWiFS Chl-a and the function shown in fig. S7. In the latter

case, OMF from B14 using the full simulation of ocean biogeochemistry is used. The variance explained by the OMF consistent with SeaWiFS Chl-a is shown in fig. S8, and the variance explained by OMF consistent with POP/BEC is shown in fig. S4. When observed distributions of Chl-a are used, B14-derived OMF performs as well as the upper end of empirical parameterizations of OMF. When POP/BEC Chl-a is used in combination with the empirical parameterizations to predict OMF, it explains significantly less variance than the B14-simulated OMF. OMF consistent with B14 explains roughly the same variance whether observed Chl-a is used as an input or the full oceanic biogeochemistry model is used. This suggests that the ability of the physically based framework used by B14 to simulate organic matter in SSA offers additional insight into the enrichment of SSA and will continue to improve as the ocean biogeochemistry model's ability to accurately simulate Chl-a improves.

Statistical analysis

Regression modeling. The relationships between predictor variables and N_d are explored using multivariate linear regressions. Here, we present the coefficients for several additional regressions. In addition to the OMF from B14 (OMF) and the sulfate concentration from the AeroCom median (SO_4), we also examine the regression based on the separation of SSA organic matter into lipid-like organic matter (LIPID) and polysaccharide-like organic matter (POLY), which have distinct seasonal and geographic patterns. Details of this partitioning are explained in section 5 (figs. S4 and S8) and in B14.

Multivariate fits to the N_d from Grosvenor and Wood (*15*) for the year 2007 with smoothed spatial interpolation (*80*, *81*) (described in greater detail below) yield the following coefficients. Uncertainties are SDs of the coefficients obtained from 10-fold cross-validation (*51*), repeated 10 times. Model results indicate that the relationship between CCN and N_d should be approximately linear in the SO (*82*), allowing the use of simple linear regression in this region.

$$\mathbf{Nd} = (115.6971 \pm 2.7742\ \mathrm{cm}^{-3})\ \mathbf{OMF} + 40.6347 \pm 0.4087\ \mathrm{cm}^{-3}$$

$$\mathbf{Nd} = (176.6927 \pm 2.4004\ \mu\mathrm{g}^{-1}\ \mathrm{m}^3\ \mathrm{cm}^{-3})\ \mathbf{SO_4} + 40.4987 \pm 0.2209\ \mathrm{cm}^{-3}$$

$$\mathbf{Nd} = (137.1134 \pm 2.5679\ \mu\mathrm{g}^{-1}\ \mathrm{m}^3\ \mathrm{cm}^{-3})\ \mathbf{SO_4} + (58.2682 \pm 1.9953\ \mathrm{cm}^{-3})\ \mathbf{OMF} + 35.6441 \pm 0.2233\ \mathrm{cm}^{-3}$$

$$\mathbf{Nd} = (139.1144 \pm 2.9050\ \mu\mathrm{g}^{-1}\ \mathrm{m}^3\ \mathrm{cm}^{-3})\ \mathbf{SO_4} + (58.0173 \pm 1.6236\ \mathrm{cm}^{-3})\ \mathbf{LIPID} + 35.9051 \pm 0.2432\ \mathrm{cm}^{-3} + (300.0160 \pm 27.1975\ \mathrm{cm}^{-3})\ \mathbf{POLY}$$

Several other predictors were investigated to rule out possible confounding variables. AeroCom SS concentration and NOAA OI SST (*72*) each predict only a small fraction of the variability in N_d (fig. S6). A linear fit to monthly mean wind speed predicted about 20 ± 10% of the variability in N_d; however, a multivariate fit including wind speed, OMF, and SO_4 concentration did not significantly increase the variance predicted by OMF and SO_4 concentration alone (fig. S9). A climatology of ocean DMS concentration (*50*) explained about 25 ± 10% of the variance in N_d (fig. S6). Although not negligible, the variance explained by each of these variables is relatively slight compared to OMF and SO_4, indicating that they are not the underlying drivers of the spatial and temporal structure of N_d in the SO, and none of these variables significantly increase predictability in a regression that also includes SO_4 and OMF.

Details of data interpolation

Regressions were performed using monthly mean N_d data averaged over 5° latitude × 15° longitude bins. Data were interpolated spatially at its native resolution and then averaged. N_d data were left blank in bins where reliable retrievals could not be made for the whole bin. Only data from oceans not covered by sea ice were used as estimated by the HADISST sea ice coverage as included in the NOAA OI SST (*72*) data.

Observations of ocean and cloud properties from space are not always possible, leading to gaps in observational data sets. SeaWiFS requires a cloud-free view of the ocean, and robust retrievals of N_d are only possible at low SZA (*15*). Resulting data gaps in N_d and observed predictor variables (Chl-a, wind speed, SST, etc.) were filled using a smoothed interpolation procedure described in (*80*, *81*). The interpolated data were then averaged in 5° latitude × 15° longitude bins. Analysis was repeated for 5° latitude × 5° longitude bins, and the variance explained was found to be fairly similar (fig. S10).

SUPPLEMENTARY MATERIALS

Supplementary material for this article is available at http://advances.sciencemag.org/cgi/content/full/1/6/e1500157/DC1

Fig. S1. The AeroCom scenario B and PRE SO_4 column density (black) across eight models (MPI-HAM excluded due to unavailability of SO_4 column density) and difference in SO_4 column density ($\mu g/m^2$) between preindustrial and present day (red).

Fig. S2. The AeroCom scenario B and PRE SO_4 surface concentration from LSCE, GISS, LOA, and UIO-GCM.

Fig. S3. The fractional change in SO_4 surface concentration between the present-day and preindustrial period from AeroCom scenario B and PRE SO_4 surface concentration from LSCE, GISS, LOA, and UIO-GCM.

Fig. S4. Tenfold cross-validation performed using only POP/BEC-modeled chlorophyll-consistent quantities.

Fig. S5. Contribution of the labile "lipid-like" group and total contribution of the semi-labile "polysaccharide-like" and "protein-like" groups to the total Nd from the regression model.

Fig. S6. The 10-fold cross-validation repeated using wind speed from the Multi-Platform Ocean Surface Wind Velocity L3.5, SST from the NOAA OI data product, SS aerosol concentration from AeroCom, and DMS (*50*).

Fig. S7. Scatter plot of lipid-like OMF in SSA as calculated by B14 as a function of POP chlorophyll.

Fig. S8. Tenfold cross-validation performed using only SeaWiFS consistent Chl-a.

Fig. S9. Tenfold cross-validation repeated using wind and SS concentration in addition to OMB14 and SO_4 concentration.

Fig. S10. As in fig. S1, but averaged over 5° latitude × 5° longitude bins.

Table S1. Correlation coefficients in space and time using labile and semi-labile fields from B14.

REFERENCES AND NOTES

1. Y. T. Hwang, D. M. W. Frierson, Link between the double-Intertropical Convergence Zone problem and cloud biases over the Southern Ocean. *Proc. Natl. Acad. Sci. U.S.A.* **110**, 4935–4940 (2013).
2. K. E. Trenberth, J. T. Fasullo, Simulation of present-day and twenty-first-century energy budgets of the Southern Oceans. *J. Climate* **23**, 440–454 (2010).
3. S. Twomey, Pollution and planetary albedo. *Atmos. Environ.* **8**, 1251–1256 (1974).
4. I. S. A. Isaksen, C. Granier, G. Myhre, T. K. Berntsen, S. B. Dalsøren, M. Gauss, Z. Klimont, R. Benestad, P. Bousquet, W. Collins, T. Cox, V. Eyring, D. Fowler, S. Fuzzi, P. Jöckel, P. Laj, U. Lohmann, M. Maione, P. Monks, A. S. H. Prevot, F. Raes, A. Richter, B. Rognerud, M. Schulz, D. Shindell, D. S. Stevenson, T. Storelvmo, W.-C. Wang, M. van Weele, M. Wild, D. Wuebbles, Atmospheric composition change: Climate–chemistry interactions. *Atmos. Environ.* **43**, 5138–5192 (2009).
5. S. J. Ghan, S. J. Smith, M. Wang, K. Zhang, K. Pringle, K. Carslaw, J. Pierce, S. Bauer, P. Adams, A simple model of global aerosol indirect effects. *J. Geophys. Res. Atmos.* **118**, 6688–6707 (2013).
6. K. S. Carslaw, L. A. Lee, C. L. Reddington, K. J. Pringle, A. Rap, P. M. Forster, G. W. Mann, D. V. Spracklen, M. T. Woodhouse, L. A. Regayre, J. R. Pierce, Large contribution of natural aerosols to uncertainty in indirect forcing. *Nature* **503**, 67–71 (2013).
7. H. Korhonen, K. S. Carslaw, D. V. Spracklen, G. W. Mann, M. T. Woodhouse, Influence of oceanic dimethyl sulfide emissions on cloud condensation nuclei concentrations and seasonality over the remote Southern Hemisphere oceans: A global model study. *J. Geophys. Res. Atmos.* **113**, D15204 (2008).
8. P. K. Quinn, T. S. Bates, The case against climate regulation via oceanic phytoplankton sulphur emissions. *Nature* **480**, 51–56 (2011).

9. A. Lana, R. Simo, S. M. Vallina, J. Dachs, Potential for a biogenic influence on cloud microphysics over the ocean: A correlation study with satellite-derived data. *Atmos. Chem. Phys.* **12**, 7977–7993 (2012).
10. R. J. Charlson, J. E. Lovelock, M. O. Andreae, S. G. Warren, Oceanic phytoplankton, atmospheric sulfur, cloud albedo and climate. *Nature* **326**, 655–661 (1987).
11. N. Meskhidze, A. Nenes, Phytoplankton and cloudiness in the Southern Ocean. *Science* **314**, 1419–1423 (2006).
12. N. Meskhidze, A. Nenes, Effects of ocean ecosystem on marine aerosol-cloud interaction. *Adv. Meteorol.* **2010**, Article ID 239808 (2010).
13. G. P. Ayers, J. L. Gras, Seasonal relationship between cloud condensation nuclei and aerosol methanesulphonate in marine air. *Nature* **353**, 834–835 (1991).
14. P. G. Falkowski, Y. Kim, Z. Kolber, C. Wilson, C. Wirick, R. Cess, Natural versus anthropogenic factors affecting low-level cloud albedo over the North Atlantic. *Science* **256**, 1311–1313 (1992).
15. D. P. Grosvenor, R. Wood, The effect of solar zenith angle on MODIS cloud optical and microphysical retrievals within marine liquid water clouds. *Atmos. Chem. Phys.* **14**, 7291–7321 (2014).
16. M. Schulz, C. Textor, S. Kinne, Y. Balkanski, S. Bauer, T. Berntsen, T. Berglen, O. Boucher, F. Dentener, S. Guibert, I. S. A. Isaksen, T. Iversen, D. Koch, A. Kirkevåg, X. Liu, V. Montanaro, G. Myhre, J. E. Penner, G. Pitari, S. Reddy, Ø. Seland, P. Stier, T. Takemura, Radiative forcing by aerosols as derived from the AeroCom present-day and pre-industrial simulations. *Atmos. Chem. Phys.* **6**, 5225–5246 (2006).
17. S. Kinne, M. Schulz, C. Textor, S. Guibert, Y. Balkanski, S. E. Bauer, T. Berntsen, T. F. Berglen, O. Boucher, M. Chin, W. Collins, F. Dentener, T. Diehl, R. Easter, J. Feichter, D. Fillmore, S. Ghan, P. Ginoux, S. Gong, A. Grini, J. Hendricks, M. Herzog, L. Horowitz, I. Isaksen, T. Iversen, A. Kirkevåg, S. Kloster, D. Koch, J. E. Kristjansson, M. Krol, A. Lauer, J. F. Lamarque, G. Lesins, X. Liu, U. Lohmann, V. Montanaro, G. Myhre, J. Penner, G. Pitari, S. Reddy, O. Seland, P. Stier, T. Takemura, X. Tie, An AeroCom initial assessment—Optical properties in aerosol component modules of global models. *Atmos. Chem. Phys.* **6**, 1815–1834 (2006).
18. O. Boucher, U. Lohmann, The sulfate-CCN-cloud albedo effect. *Tellus B* **47**, 281–300 (1995).
19. A. Jones, D. L. Roberts, A. Slingo, A climate model study of indirect radiative forcing by anthropogenic sulfate aerosols. *Nature* **370**, 450–453 (1994).
20. D. A. Hegg, Y. J. Kaufman, Measurements of the relationship between submicron aerosol number and volume concentration. *J. Geophys. Res. Atmos.* **103**, 5671–5678 (1998).
21. D. A. Knopf, P. A. Alpert, B. Wang, J. Y. Aller, Stimulation of ice nucleation by marine diatoms. *Nat. Geosci.* **4**, 88–90 (2011).
22. S. M. Burrows, C. Hoose, U. Pöschl, M. G. Lawrence, Ice nuclei in marine air: Biogenic particles or dust? *Atmos. Chem. Phys.* **13**, 245–267 (2013).
23. T. D. Jickells, Z. S. An, K. K. Andersen, A. R. Baker, G. Bergametti, N. Brooks, J. J. Cao, P. W. Boyd, R. A. Duce, K. A. Hunter, H. Kawahata, N. Kubilay, J. laRoche, P. S. Liss, N. Mahowald, J. M. Prospero, A. J. Ridgwell, I. Tegen, R. Torres, Global iron connections between desert dust, ocean biogeochemistry, and climate. *Science* **308**, 67–71 (2005).
24. N. M. Mahowald, S. Engelstaedter, C. Luo, A. Sealy, P. Artaxo, C. Benitez-Nelson, S. Bonnet, Y. Chen, P. Y. Chuang, D. D. Cohen, F. Dulac, B. Herut, A. M. Johansen, N. Kubilay, R. Losno, W. Maenhaut, A. Paytan, J. M. Prospero, L. M. Shank, R. L. Siefert, Atmospheric iron deposition: Global distribution, variability, and human perturbations. *Ann. Rev. Mar. Sci.* **1**, 245–278 (2009).
25. R. B. Husar, J. M. Prospero, L. L. Stowe, Characterization of tropospheric aerosols over the oceans with the NOAA advanced very high resolution radiometer optical thickness operational product. *J. Geophys. Res. Atmos.* **102**, 16889–16909 (1997).
26. D. M. Murphy, J. R. Anderson, P. K. Quinn, L. M. McInnes, F. J. Brechtel, S. M. Kreidenweis, A. M. Middlebrook, M. Pósfai, D. S. Thomson, P. R. Buseck, Influence of sea-salt on aerosol radiative properties in the Southern Ocean marine boundary layer. *Nature* **392**, 62–65 (1998).
27. J. M. Prospero, P. Ginoux, O. Torres, S. E. Nicholson, T. E. Gill, Environmental characterization of global sources of atmospheric soil dust identified with the nimbus 7 Total Ozone Mapping Spectrometer (TOMS) absorbing aerosol product. *Rev. Geophys.* **40**, 1002 (2002).
28. F. Dentener, S. Kinne, T. Bond, O. Boucher, J. Cofala, S. Generoso, P. Ginoux, S. Gong, J. J. Hoelzemann, A. Ito, L. Marelli, J. E. Penner, J.-P. Putaud, C. Textor, M. Schulz, G. R. van der Werf, J. Wilson, Emissions of primary aerosol and precursor gases in the years 2000 and 1750 prescribed data-sets for AeroCom. *Atmos. Chem. Phys.* **6**, 4321–4344 (2006).
29. S. M. Vallina, R. Simó, S. Gassó, What controls CCN seasonality in the Southern Ocean? A statistical analysis based on satellite-derived chlorophyll and CCN and model-estimated OH radical and rainfall. *Global Biogeochem. Cycles* **20**, GB1014 (2006).
30. N. Huneeus, M. Schulz, Y. Balkanski, J. Griesfeller, J. Prospero, S. Kinne, S. Bauer, O. Boucher, M. Chin, F. Dentener, T. Diehl, R. Easter, D. Fillmore, S. Ghan, P. Ginoux, A. Grini, L. Horowitz, D. Koch, M. C. Krol, W. Landing, X. Liu, N. Mahowald, R. Miller, J.-J. Morcrette, G. Myhre, J. Penner, J. Perlwitz, P. Stier, T. Takemura, C. S. Zender, Global dust model intercomparison in AeroCom phase I. *Atmos. Chem. Phys.* **11**, 7781–7816 (2011).
31. V. A. Karydis, P. Kumar, D. Barahona, I. N. Sokolik, A. Nenes, On the effect of dust particles on global cloud condensation nuclei and cloud droplet number. *J. Geophys. Res. Atmos.* **116**, D23204 (2011).
32. P. K. Quinn, T. S. Bates, K. S. Schulz, D. J. Coffman, A. A. Frossard, L. M. Russell, W. C. Keene, D. J. Kieber, Contribution of sea surface carbon pool to organic matter enrichment in sea spray aerosol. *Nat. Geosci.* **7**, 228–232 (2014).
33. A. A. Frossard, L. M. Russell, S. M. Burrows, S. M. Elliott, T. S. Bates, P. K. Quinn, Sources and composition of submicron organic mass in marine aerosol particles. *J. Geophys. Res. Atmos.* **119**, 12977–13003 (2014).
34. M. C. Facchini, M. Rinaldi, S. Decesari, C. Carbone, E. Finessi, M. Mircea, S. Fuzzi, D. Ceburnis, R. Flanagan, E. D. Nilson, G. de Leeuw, M. Martino, J. Woeltjen, C. D. O'Dowd, Primary submicron marine aerosol dominated by insoluble organic colloids and aggregates. *Geophys. Res. Lett.* **35**, L17814 (2008).
35. E. K. Bigg, Sources, nature and influence on climate of marine airborne particles. *Environ. Chem.* **4**, 155–161 (2007).
36. E. K. Bigg, C. Leck, The composition of fragments of bubbles bursting at the ocean surface. *J. Geophys. Res. Atmos.* **113**, D11209 (2008).
37. L. N. Hawkins, L. Russell, Polysaccharides, proteins, and phytoplankton fragments: Four chemically distinct types of marine primary organic aerosol classified by single particle spectromicroscopy. *Adv. Meteorol.* **2010**, Article ID 612132 (2010).
38. L. M. Russell, L. N. Hawkins, A. A. Frossard, P. K. Quinn, T. S. Bates, Carbohydrate-like composition of submicron atmospheric particles and their production from ocean bubble bursting. *Proc. Natl. Acad. Sci. U.S.A.* **107**, 6652–6657 (2010).
39. V. C. Turekian, S. A. Macko, W. C. Keene, Concentrations, isotopic compositions, and sources of size-resolved, particulate organic carbon and oxalate in near-surface marine air at Bermuda during spring. *J. Geophys. Res. Atmos.* **108**, 4157 (2003).
40. M. Rinaldi, S. Decesari, C. Carbone, E. Finessi, S. Fuzzi, D. Ceburnis, C. D. O'Dowd, J. Sciare, J. P. Burrows, M. vrekoussis, B. Ervens, K. Tsigaridis, M. C. Facchini, Evidence of a natural marine source of oxalic acid and a possible link to glyoxal. *J. Geophys. Res. Atmos.* **116**, D16204 (2011).
41. S. R. Arnold, D. V. Spracklen, J. Williams, N. Yassaa, J. Sciare, B. Bonsang, V. Gros, I. Peeken, A. C. Lewis, S. Alvain, C. Moulin, Evaluation of the global oceanic isoprene source and its impacts on marine organic carbon aerosol. *Atmos. Chem. Phys.* **9**, 1253–1262 (2009).
42. X. Zhou, A. J. Davis, D. J. Kieber, W. C. Keene, J. R. Maben, H. Maring, E. E. Dahl, M. A. Izaguirre, R. Sander, L. Smoydzyn, Photochemical production of hydroxyl radical and hydroperoxides in water extracts of nascent marine aerosols produced by bursting bubbles from Sargasso seawater. *Geophys. Res. Lett.* **35**, L20803 (2008).
43. S. M. Burrows, O. Ogunro, A. A. Frossard, L. M. Russell, P. J. Rasch, S. M. Elliott, A physically based framework for modeling the organic fractionation of sea spray aerosol from bubble film Langmuir equilibria. *Atmos. Chem. Phys.* **14**, 13601–13629 (2014).
44. R. T. Letscher, J. K. Moore, Y. C. Teng, F. Primeau, Variable C : N : P stoichiometry of dissolved organic matter cycling in the Community Earth System Model. *Biogeosciences* **12**, 209–221 (2015).
45. S. C. Doney, I. Lima, J. K. Moore, K. Lindsay, M. J. Behrenfeld, T. K. Westberry, N. Mahowald, D. M. Glover, T. Takahashi, Skill metrics for confronting global upper ocean ecosystem-biogeochemistry models against field and remote sensing data. *J. Mar. Syst.* **76**, 95–112 (2009).
46. D. M. Westervelt, R. H. Moore, A. Nenes, P. J. Adams, Effect of primary organic sea spray emissions on cloud condensation nuclei concentrations. *Atmos. Chem. Phys.* **12**, 89–101 (2012).
47. M. S. Long, W. C. Keene, D. J. Kieber, A. A. Frossard, L. M. Russell, J. R. Maben, J. D. Kinsey, P. K. Quinn, T. S. Bates, Light-enhanced primary marine aerosol production from biologically productive seawater. *Geophys. Res. Lett.* **41**, 2661–2670 (2014).
48. W. C. Keene, H. Maring, J. R. Maben, D. J. Kieber, A. A. P. Pszenny, E. E. Dahl, M. A. Izaguirre, A. J. Davis, M. S. Long, X. Zhou, L. Smoydzin, R. Sander, Chemical and physical characteristics of nascent aerosols produced by bursting bubbles at a model air-sea interface. *J. Geophys. Res. Atmos.* **112** (2007).
49. M. S. Long, W. C. Keene, D. J. Kieber, D. J. Erickson, H. Maring, A sea-state based source function for size- and composition-resolved marine aerosol production. *Atmos. Chem. Phys.* **11**, 1203–1216 (2011).
50. A. Lana, T. G. Bell, R. Simó, S. M. Vallina, J. Ballabrera-Poy, A. J. Kettle, J. Dachs, L. Bopp, E. S. Saltzman, J. Stefels, J. E. Johnson, P. S. Liss, An updated climatology of surface dimethlysulfide concentrations and emission fluxes in the global ocean. *Global Biogeochem. Cycles* **25**, GB1004 (2011).
51. R. Kohavi, paper presented at the Proceedings of the 14th International Joint Conference on Artificial Intelligence—Volume 2, Montreal, Quebec, Canada, 1995.
52. R. Boers, J. B. Jensen, P. B. Krummel, Microphysical and short-wave radiative structure of stratocumulus clouds over the Southern Ocean: Summer results and seasonal differences. *Q. J. R. Meteorol. Soc.* **124**, 151–168 (1998).
53. J. L. Gras, Cloud condensation nuclei over the Southern Ocean. *Geophys. Res. Lett.* **17**, 1565–1567 (1990).
54. A. Schmidt, K. S. Carslaw, G. W. Mann, A. Rap, K. J. Pringle, D. V. Spracklen, M. Wilson, P. M. Forster, Importance of tropospheric volcanic aerosol for indirect radiative forcing of climate. *Atmos. Chem. Phys.* **12**, 7321–7339 (2012).
55. A. Rap, C. E. Scott, D. V. Spracklen, N. Bellouin, P. M. Forster, K. S. Carslaw, A. Schmidt, G. Mann, Natural aerosol direct and indirect radiative effects. *Geophys. Res. Lett.* **40**, 3297–3301 (2013).

56. S. Kloster, J. Feichter, E. Maier-Reimer, K. D. Six, P. Stier, P. Wetze, DMS cycle in the marine ocean-atmosphere system—A global model study. *Biogeosciences* **3**, 29–51 (2006).
57. D. T. McCoy, D. L. Hartmann, D. P. Grosvenor, Observed Southern Ocean cloud properties and shortwave reflection. Part II: Phase changes and low cloud feedback. *J. Climate* **27**, 8858–8868 (2014).
58. A. J. Conley, J. F. Lamarque, F. Vitt, W. D. Collins, J. Kiehl, PORT, a CESM tool for the diagnosis of radiative forcing. *Geosci. Model Dev.* **6**, 469–476 (2013).
59. M. A. Thomas, P. Suntharalingam, L. Pozzoli, S. Rast, A. Devasthale, S. Kloster, J. Feichter and T. M. Lenton, Quantification of DMS aerosol-cloud-climate interactions using ECHAM5-HAMMOZ model in current climate scenario. *Atmos. Chem. Phys. Discuss.* **10**, 3087–3127 (2010).
60. D. T. McCoy, D. L. Hartmann, D. P. Grosvenor, Observed Southern Ocean cloud properties and shortwave reflection. Part I: Calculation of SW flux from observed cloud properties. *J. Clim.* **27**, 8836–8857 (2014).
61. M. D. Zelinka, T. Andrews, P. M. Forster, K. E. Taylor, Quantifying components of aerosol-cloud-radiation interactions in climate models. *J. Geophys. Res. Atmos.* **119**, 7599–7615 (2014).
62. A. Engstrom, F. A. M. Bender, R. J. Charlson, R. Wood, *Geographically coherent patterns of albedo enhancement and suppression associated with aerosol sources and sinks*. *Tellus* **67**, 26442 (2015).
63. K. A. Prather, T. H. Bertram, V. H. Grassian, G. B. Deane, M. D. Stokes, P. J. DeMott, L. I. Aluwihare, B. P. Palenik, F. Azam, J. H. Seinfeld, R. C. Moffet, M. J. Molina, C. D. Cappa, F. M. Geiger, G. C. Roberts, L. M. Russell, A. P. Ault, J. Baltrusaitis, D. B. Collins, C. E. Corrigan, L. A. Cuadra-Rodriguez, C. J. Ebben, S. D. Forestieri, T. L. Guasco, S. P. Hersey, M. J. Kim, W. F. Lambert, R. L. Modini, W. Mui, B. E. Pedler, M. J. Ruppel, O. S. Ryder, N. G. Schoepp, R. C. Sullivan, and D. Zhao, Bringing the ocean into the laboratory to probe the chemical complexity of sea spray aerosol. *Proc. Natl. Acad. Sci. U.S.A.* **110**, 7550–7555 (2013).
64. A. P. Ault, R. C. Moffet, J. Baltrusaitis, D. B. Collins, M. J. Ruppel, L. A. Cuadra-Rodriguez, D. Zhao, T. L. Guasco, C. J. Ebben, F. M. Geiger, T. H. Bertram, K. A. Prather, V. H. Grassian, Size-dependent changes in sea spray aerosol composition and properties with different seawater conditions. *Environ. Sci. Technol.* **47**, 5603–5612 (2013).
65. J. Ovadnevaite, D. Ceburnis, G. Martucci, J. Bialek, C. Monahan, M. Rinaldi, M. C. Facchini, H. Berresheim, D. R. Worsnop, C. O'Dowd, Primary marine organic aerosol: A dichotomy of low hygroscopicity and high CCN activity. *Geophys. Res. Lett.* **38**, L21806 (2011).
66. H. Kokkola, R. Sorjamaa, A. Peraniemi, T. Raatikainen, A. Laaksonen, Cloud formation of particles containing humic-like substances. *Geophys. Res. Lett.* **33**, L10816 (2006).
67. C. D. O'Dowd, M. C. Facchini, F. Cavalli, D. Ceburnis, M. Mircea, S. Decesari, S. Fuzzi, Y. J. Yoon, J. P. Putaud, Biogenically driven organic contribution to marine aerosol. *Nature* **431**, 676–680 (2004).
68. J. Sciare, O. Favez, R. Sarda-Estève, K. Oikonomou, H. Cachier, V. Kazan, Long-term observations of carbonaceous aerosols in the Austral Ocean atmosphere: Evidence of a biogenic marine organic source. *J. Geophys. Res. Atmos.* **114**, D15302 (2009).
69. R. L. Modini, G. R. Johnson, C. R. He, Z. D. Ristovski, Observation of the suppression of water uptake by marine particles. *Atmos. Res.* **98**, 219–228 (2010).
70. D. B. Collins, A. P. Ault, R. C. Moffet, M. J. Ruppel, L. A. Cuadra-Rodriguez, T. L. Guasco, C. E. Corrigan, B. E. Pedler, F. Azam, L. I. Aluwihare, T. H. Bertram, G. C. Roberts, V. H. Grassian, K. A. Prather, Impact of marine biogeochemistry on the chemical mixing state and cloud forming ability of nascent sea spray aerosol. *J. Geophys. Res. Atmos.* **118**, 8553–8565 (2013).
71. A. A. Lacis, J. Hansen, A parameterization for the absorption of solar radiation in the Earth's atmosphere. *J. Atmos. Sci.* **31**, 118–133 (1974).
72. R. W. Reynolds, N. A. Rayner, T. M. Smith, D. C. Stokes, W. Wang, An improved in situ and satellite SST analysis for climate. *J. Climate* **15**, 1609–1625 (2002).
73. J. W. Hurrell, M. M. Holland, P. R. Gent, S. Ghan, J. E. Kay, P. J. Kushner, J.-F. Lamarque, W. G. Large, D. Lawrence, K. Lindsay, W. H. Lipscomb, M. C. Long, N. Mahowald, D. R. Marsh, R. B. Neale, P. Rasch, S. Vavrus, M. Vertenstein, D. Bader, W. D. Collins, J. J. Hack, J. Kiehl, and S. Marshall, The Community Earth System Model: A framework for collaborative research. *Bull. Am. Meteorol. Soc.* **94**, 1339–1360 (2013).
74. R. B. Neale, Description of the NCAR Community Atmosphere Model (CAM 5.0) (2010).
75. E. J. Mlawer, S. J. Taubman, P. D. Brown, M. J. Iacono, S. A. Clough, Radiative transfer for inhomogeneous atmospheres: RRTM, a validated correlated-k model for the longwave. *J. Geophys. Res. Atmos.* **102**, 16663–16682 (1997).
76. H. Morrison, A. Gettelman, A new two-moment bulk stratiform cloud microphysics scheme in the Community Atmosphere Model, version 3 (CAM3). Part I: Description and numerical tests. *J. Climate* **21**, 3642–3659 (2008).
77. I. C. Tsai, J. P. Chen, P. Y. Lin, W. C. Wang, I. S. A. Isaksen, Sulfur cycle and sulfate radiative forcing simulated from a coupled global climate-chemistry model. *Atmos. Chem. Phys.* **10**, 3693–3709 (2010).
78. C. Textor, M. Schulz, S. Guibert, S. Kinne, Y. Balkanski, S. Bauer, T. Berntsen, T. Berglen, O. Boucher, M. Chin, F. Dentener, T. Diehl, R. Easter, H. Feichter, D. Fillmore, S. Ghan, P. Ginoux, S. Gong, A. Grini, J. Hendricks, L. Horowitz, P. Huang, I. Isaksen, I. Iversen, S. Kloster, D. Koch, A. Kirkevåg, J. E. Kristjansson, M. Krol, A. Lauer, J. F. Lamarque, X. Liu, V. Montanaro, G. Myhre, J. Penner, G. Pitari, S. Reddy, Ø. Seland, P. Stier, T. Takemura, and X. Tie, Analysis and quantification of the diversities of aerosol life cycles within AeroCom. *Atmos. Chem. Phys.* **6**, 1777–1813 (2006).
79. B. Gantt, N. Meskhidze, M. C. Facchini, M. Rinaldi, D. Ceburnis, and C. D. O'Dowd, Wind speed dependent size-resolved parameterization for the organic mass fraction of sea spray aerosol. *Atmos. Chem. Phys.* **11**, 8777–8790 (2011).
80. D. Garcia, Robust smoothing of gridded data in one and higher dimensions with missing values. *Comput. Stat. Data Anal.* **54**, 1167–1178 (2010).
81. G. J. Wang, D. Garcia, Y. Liu, R. de Jeu, A. J. Dolman, A three-dimensional gap filling method for large geophysical datasets: Application to global satellite soil moisture observations. *Environ. Model. Software* **30**, 139–142 (2012).
82. K. J. Pringle, K. S. Carslaw, D. V. Spracklen, G. M. Mann, M. P. Chipperfield, The relationship between aerosol and cloud drop number concentrations in a global aerosol microphysics model. *Atmos. Chem. Phys. Discuss.* **9**, 3207–3241 (2009).

Acknowledgments: We wish to thank the AeroCom intercomparison project for making the sea salt and sulfate model median data used in this study available, and the modeling centers whose models constitute the median data set: UMI, UIO-CTM, LOA, LSCE, MPI-HAM, GISS, UIO-GCM, SPRINTARS, and ULAQ. CERES data were obtained from the NASA Langley Research Center CERES ordering tool. MODIS data were obtained from the NASA Goddard Land Processes data archive. We thank A. Conley and F. Vitt for assistance setting up the PORT offline radiative transfer calculations; M. Maltrud for providing the POP/BEC ocean biogeochemistry simulation data underlying the B14 parameterization; and B. Singh for technical support at PNNL. We also wish to thank the three anonymous reviewers, R. Charlson, C. Gaston, A. McCoy, and J. McCoy, for useful discussion and advice. POP/BEC, PORT, and CAM5 are components of the Community Earth System Model (CESM). The CESM project is supported by the National Science Foundation and the Office of Science of the U.S. Department of Energy. The PORT radiative transfer calculations were performed using EMSL, a DOE Office of Science User Facility sponsored by the Office of Biological and Environmental Research (BER) and located at Pacific Northwest National Laboratory. **Funding:** We wish to acknowledge the following funding sources: D.L.H. and D.T.M. were supported under NASA Grant NNX14AG26G, and D.T.M. acknowledges government support awarded by DoD, Air Force Office of Scientific Research, National Defense Science and Engineering Graduate (NDSEG) Fellowship, 32 CFR 168a. S.M.B., P.-L.M., and P.J.R. were supported by the U.S. Department of Energy, Office of Science, BER as part of the Earth System Modeling program. D.P.G. was supported by the School of Earth and Environment at the University of Leeds. R.W. was supported by NASA Grant NNX13AQ35G. S.M.E. was supported by several DOE SciDAC and SFA earth system modeling projects (Scientific Discovery through Advanced Computing, Science Focus Areas). **Author contributions:** D.T.M. and S.M.B. performed analysis and prepared figures and the manuscript. R.W., D.P.G., S.M.E., P.-L.M., P.J.R., and D.L.H. assisted with the analyses and preparation of the manuscript. All authors proofread and corrected the final version. **Competing interests:** The authors declare that they have no competing interests.

Submitted 4 February 2015
Accepted 7 May 2015
Published 17 July 2015
10.1126/sciadv.1500157

Citation: D. T. McCoy, S. M. Burrows, R. Wood, D. P. Grosvenor, S. M. Elliott, P.-L. Ma, P. J. Rasch, D. L. Hartmann, Natural aerosols explain seasonal and spatial patterns of Southern Ocean cloud albedo. *Sci. Adv.* **1**, e1500157 (2015).